Medium effects in K^+ nuclear interactions *

E. Friedman[a], A. Gal[a], J. Mareš[b]

[a] *Racah Institute of Physics, The Hebrew University, Jerusalem 91904, Israel*

[b] *Nuclear Physics Institute, 25068 Řež, Czech Republic*

Abstract

Total (σ_T) and reaction (σ_R) cross sections are derived self consistently from the attenuation cross sections measured in transmission experiments at the AGS for K^+ on ^{6}Li, C, Si and Ca in the momentum range of 500-700 MeV/c by using a $V_{opt} = t_{eff}(\rho)\rho$ optical potential. Self consistency requires, for the KN in-medium t matrix, that Im $t_{eff}(\rho)$ increases linearly with the average nuclear density in excess of a threshold value of 0.088 ± 0.004 fm^{-3}. The density dependence of Re $t_{eff}(\rho)$ is studied phenomenologically, and also applying a relativistic mean field approach, by fitting to the σ_T and σ_R values. The real part of the optical potential is found to be systematically less repulsive with increasing energy than expected from the free-space repulsive KN interaction. When the elastic scatttering data for ^{6}Li and C at 715 MeV/c are included in the analysis, a tendency of Re V_{opt} to generate an attractive pocket at the nuclear surface is observed.

PACS: 25.80.Nv; 13.85.Lg; 13.75.-n; 21.30.Fe

Keywords: K^+ nucleus total and reaction cross sections 500-700 MeV/c on ^{6}Li, C, Si, Ca; Self consistent analysis; Medium effects.

*Dedicated to the memory of Carl Dover, a friend, colleague and scholar.

I. INTRODUCTION

The KN interaction for incoming momenta up to 1 GeV/c is fairly weak, with typical total cross reaction values of 10-15 mb. It is expected then [1] that K-nuclear interactions be well described, in terms of the free-space KN t matrix and the nuclear density ρ, by the first-order optical potential $V_{opt} = t\rho$. However, K^+ nucleus total cross section values [2–7] and reaction cross section values [7] derived from attenuation cross sections measured in transmission experiments, as well as elastic [8,9] and inelastic differential cross sections [8,10] and quasifree spectra [11], all point to a substantial departure of the order of 10-20% from the predictions of a simple $t\rho$ potential, even when many conventional nuclear medium effects are incorporated [12,13]. Several nonconventional medium effects have also been proposed to remedy the failure of the first-order optical potential approach, such as nucleon swelling [14], or density dependent vector meson masses [15], or polarizing the nuclear medium by $\bar{\mathrm{N}}\mathrm{N}$ excitations [16], or meson exchange currents [17,18], but as we shall discuss in the concluding section, none of these models provides a satisfactory solution to the discrepancy.

It was pointed out by Friedman et al. [7] that values of σ_R and σ_T derived from transmission measurements are not model independent. Indeed a knowledge of the Coulomb-nuclear interference contribution at small angles is required in order to extrapolate these measurements to zero degrees, where the total and reaction cross sections are determined. Traditionally, an optical potential is assumed for the purpose of extrapolation, even though it is not guaranteed that a particularly chosen V_{opt} yields by calculation the same values of σ_R and σ_T which eventually are derived by using it throughout the extrapolation of the data. In this sense, most existing derivations of total cross sections in the literature do not satisfy the basic requirement of *self consistency*. The question of self consistency, posed for V_{opt}, is whether or not optical potentials which are constructed empirically to fit σ_R and σ_T values derived from transmission experiments lead to the same values, within errors, when used in reanalyzing these same experiments. Friedman, Gal and Mareš [19] have recently discussed

this issue, showing that self consistency for K^+ nucleus cross sections can be achieved by using a density dependent optical potential $V_{opt} = t_{eff}(\rho)\rho$ with Im $t_{eff}(\rho)$ depending linearly on the average density in excess of a threshold value.

In this paper we report σ_T and σ_R values for K^+ interactions with ^{6}Li, C, Si and Ca, as derived self consistently from the attenuation cross sections measured in transmission experiments [6] at the AGS, at 488, 531, 656 and 714 MeV/c. Previous background as well as a preliminary report for 714 MeV/c is given in Ref. [19]. Section II describes the wave equation and the optical potentials used in analyzing the data and Section III summarizes the reaction and total cross sections obtained from a self consistent analysis of the transmission measurements. The phenomenology of Re V_{opt} is discussed in Section IV, by studying its density dependence. Some of the calculations include also fits to the angular distribution data of Ref. [9]. A relativistic mean field approach to Re V_{opt} is presented in Section V. Both approaches suggest that Re V_{opt} becomes less repulsive with increasing energy than expected from the free-space repulsive KN t matrix interaction. Section VI consists of a summary and discussion.

II. OPTICAL POTENTIALS

Following Ref. [19], the interaction of K^+ with nuclei is described in the present work by the Klein Gordon equation

$$\left[\nabla^2 + k^2 - (2\varepsilon_{red}^{(A)} V - V_c^2)\right]\psi = 0 \quad (\hbar = c = 1) \tag{1}$$

where k and $\varepsilon_{red}^{(A)}$ are the wave number and reduced energy respectively in the c.m. system, $(\varepsilon_{red}^{(A)})^{-1} = E_p^{-1} + E_t^{-1}$ in terms of the c.m. energies for the projectile and target particles, respectively. V_c is the Coulomb potential due to the charge distribution of the nucleus, and $V = V_c + V_{opt}$. The simplest possible $t\rho$ form for the optical potential is

$$2\varepsilon_{red}^{(A)} V_{opt}(r) = -4\pi F_k b_0 \rho(r), \qquad F_k = \frac{M_A\sqrt{s}}{M(E_t + E_p)} \quad , \tag{2}$$

where F_k is a kinematical factor resulting from the transformation of amplitudes between the KN and the K^+ nucleus c.m. systems and b_0 is the value of the KN scattering amplitude in the forward direction. M is the free nucleon mass, M_A is the mass of the target nucleus, $\sqrt{s}$ is the total projectile-nucleon energy in their c.m. system and the nuclear density distribution $\rho(r)$ is normalized to A, the number of nucleons in the target nucleus. It is instructive to note that, in the eikonal approximation, the probability attenuation produced by the potential (2) for the propagation law implied by using the wave equation (1) (for $V_c = 0$) is given by

$$|\psi_{eik}(b,z)|^2 \Big/ |\psi_{eik}(b,-\infty)|^2 = \exp\left(-\sigma \int_{-\infty}^{z} \rho(b,\zeta)\, d\zeta\right) , \tag{3}$$

where σ is the KN total cross section. Eq.(3) corresponds to a semiclassical picture of the K^+ projectile propagating forward with a mean free path $(\sigma\rho)^{-1}$ in a medium of density ρ, thus justifying the use of the wave equation (1) with $V_{opt} = t\rho$ of Eq.(2). Other relativistic wave equations were tested for comparison in Refs. [7,19] and yielded cross section values practically the same within few percents as those presented here. As for our final conclusions, details do slightly change using other wave equations, but the overall picture remains unchanged.

A convenient 'macroscopic' (MAC) parameterization of nuclear densities is in terms of a 2- or 3- parameter Fermi function or, for light nuclei, in terms of a modified harmonic oscillator density. Experimental information on nuclear charge densities is often presented using these functions [20], and the proton densities may then be obtained by properly unfolding the finite size of the proton. Such densities are adequate around the nuclear surface where the root-mean-square (r.m.s.) radius is determined. However, such distributions cannot be valid far outside the nucleus because they do not possess the correct exponential fall-off, as determined by the binding energy of the least bound particles. In that region it is more appropriate to use single-particle (SP) densities or densities obtained from a more realistic Hartree-Fock (HF) calculation. A convenient way for generating 'microscopic' or SP nuclear densities is to fill the appropriate single particle levels in a Woods-Saxon potential (sepa-

rately for protons and neutrons). The radius parameter of the potential is then adjusted so that the resulting proton density distribution reproduces the r.m.s. radius of the charge distribution (after folding in the finite size of the proton) whilst at the same time the depth of the potential is adjusted so that the binding energy of the least bound particle is set to the corresponding separation energy, thus ensuring the correct fall-off of the density at large radii. Using this method, which is obviously a simplification, rather realistic density distributions are obtained, particularly outside the nuclear surface. The two models, namely the MAC and the SP models, will be used here.

Fits to the data may be made by adjusting a complex parameter t_{eff} which is related to an effective forward scattering amplitude b_{eff} as follows:

$$2\varepsilon_{red}^{(A)} t_{eff} = -4\pi F_k b_{eff} \quad . \tag{4}$$

In Ref. [19] it was shown that very good *self consistent* fits to the data could be obtained if the imaginary part of t_{eff} was made density dependent according to the empirical expression:

$$t_{eff}(\rho) = \mathrm{Re}\ t_{eff} + i\mathrm{Im}\ t_{eff}\,[1 + \beta(\overline{\rho} - \rho_{th})\Theta(\overline{\rho} - \rho_{th})] \quad , \tag{5}$$

where the average nuclear density is defined as follows:

$$\overline{\rho} = \frac{1}{A}\int \rho^2 d\mathbf{r}. \tag{6}$$

Values of $\overline{\rho}$ can be obtained from HF calculations or from the simpler SP calculations described above. Results for the four nuclei of the present work are given in Table I, where the uncertainties for C, Si and Ca are about 1%. It was found that the values

$$\beta = (13.0 \pm 3.4)\ \mathrm{fm}^3 \quad , \qquad \rho_{th} = (0.088 \pm 0.004)\ \mathrm{fm}^{-3} \quad , \tag{7}$$

provide excellent self consistent fits at all four momenta for which transmission measurements on ^{6}Li, C, Si and Ca were made at the AGS [3–6]. Attempting to avoid the use of a threshold density ρ_{th} in Eq.(5) by using powers of the average or local density $\rho(r)$ failed to produce fits to the data. Note that the value of the threshold density (Eq.(7)) is considerably larger

than the average density of ^{6}Li, while comfortably smaller than $\overline{\rho}$ of the other target nuclei. This reflects the failure to reconcile the ^{6}Li data with the data for the denser nuclei, unless the specific density dependence given by Eq.(5) is assumed. This density dependence, for the parameters of Eq.(7), amounts to 20-30% enhancement, depending on the nucleus.

Results of the self consistent fits are given in Table II, essentially taken from Ref. [19]. Listed are values of the fitted KN effective forward scattering amplitude b_{eff} which are determined exclusively by fitting to the ^{6}Li data. It was demonstrated in Ref. [19] that in the present incoming momentum range, and for a KN interaction strength as weak as here encountered, using an optical potential to describe scattering off as light a nucleus as ^{6}Li incurs errors of no larger than 2%. With respect to the free-space KN scattering amplitude b_0, the values listed for Im b_{eff} show enhancement of 5-15% with increasing momentum, in quantitative agreement with the estimates of meson exchange currents effects [18]. The values listed for Re b_{eff} show a considerably larger departure. The KN in-medium t_{eff} is substantially less repulsive than the free-space t. It was pointed out in Ref. [19] that such a trend might be expected partly due to the proximity of the K*N and KΔ channels, but no quantitative estimates of this effect have been made.

III. INTEGRAL CROSS SECTIONS FROM TRANSMISSION MEASUREMENTS

As explained above and in Ref. [19], we have succeeded in obtaining self consistency in the analysis of transmission experiments by rescaling the imaginary part of the optical potential with the *average* nuclear density above a threshold value. No explanation could be given to this empirical result, but we note that with such a rescaling, which was found to be independent of beam momentum, we are able to obtain reaction and total cross sections which are consistent with the optical potential used to extract these quantities from the results of transmission measurements. Table III summarizes the reaction and total cross sections at the four beam momenta. The uncertainties are the same as quoted in the earlier publication [7], and they reflect statistical errors only. Systematic uncertainties are

associated mostly with the optical model input which is inherent in the analysis [21,7]. These were estimated to be as large as 5-10%. Indeed it can be seen that the results in Table III differ from those of Ref. [7] by about 5%, always exceeding the previous values.

IV. PHENOMENOLOGY OF THE REAL POTENTIAL

The modification of the conventional optical potential, which made possible the self consistent analysis and consequently led to the reasonably good fits to the data, was the introduction of rescaling of the imaginary potential with the factor $1+\beta(\overline{\rho}-\rho_{th})\Theta(\overline{\rho}-\rho_{th})$. In addition to this peculiar behaviour of the imaginary potential it is seen from Table II that systematic trends can be obtained from the real part of the best fit potentials. More specifically, the real part of the optical potential is found to be less repulsive than what is expected from the $t\rho$ model. The loss of repulsion seems to grow with increasing momentum, and at the two highest momenta the real part of the potential is essentially consistent with zero. To study further the real part of the optical potential we introduce a phenomenological density dependence (DD) also into the real potential such that the real part of t_{eff} is made to depend on the nuclear density as follows:

$$b_{eff} \longrightarrow b_{eff} + B_0 \left[\frac{\rho(r)}{\rho(0)}\right]^{\alpha}. \tag{8}$$

This form of a potential was found to be quite successful in studies of DD effects in kaonic atoms [22] and in Σ^- atoms [23,24]. It must be emphasized that this is a purely phenomenological form and that no significance is attached to e.g. the exponent α. However, when b_{eff} is constrained to have the corresponding value b_0 for the free-space KN interaction and when $\alpha > 0$, then the low density limit [25] is respected by the real potential. Using such a DD potential for the real part and using the same form, Eq.(5), for the imaginary potential (varying only Im b_{eff}), we performed χ^2 fits, separately at each energy, to the reaction and total cross sections of Table III. In the left hand side of Table IV are given the parameters of the real potential from unconstrained fits, where Re b_{eff}, Im b_{eff}, Re B_0 and α were

varied. Fits of similar quality could be obtained for a wide range of values for α and the results shown here are for $\alpha = 2$. The errors quoted are obtained from the χ^2 fit procedure and in this case there are strong correlations between Re b_{eff} and Re B_0. Some decrease in the values of χ^2 compared to the corresponding values in Table II is evident. In the right hand side of Table IV are given the results of constrained fits, as explained above. This time the value of α, which again was held fixed during the fits, was 0.5 as it gave slightly better results. In this case there are no correlation effects and the errors of Re B_0 apply to the sum of Re b_0 and Re B_0. This sum can be compared directly to the values of the density independent parameter Re b_{eff} of Table II. It is seen that the two sets of numbers agree remarkably well, thus supporting the preliminary conclusions from Table II regarding the real part of the potential.

Comparing the results of the two kinds of fits in Table IV, there is a distinct difference regarding the behaviour of the real potential at large radii. Whereas the constrained fit is dominated by the free-space KN interaction at large radii and consequently is repulsive at all four momenta of the present study, the unconstrained fit leads nominally to an attractive potential at large radii for 656 and 714 MeV/c. A way of bypassing the problem of correlations between errors is to apply a 'notch test' method [26] to estimate the uncertainties in the real potential as a function of position. Figure 1 shows the real part of the optical potential for 714 MeV/c K^+ on carbon as obtained from the unconstrained fits, together with the errors from the notch test. Obviously more data is needed in order to study the real potential.

Differential cross sections for the elastic scattering of K^+ by ^{6}Li and C are available at the highest momentum covered by the transmission measurements [9] and it is therefore possible to include them in the optical model fits. The adequacy of the optical potential Eq.(2) was tested by comparing angular distributions calculated for this potential with angular distributions calculated for an equivalent potential [7] containing an explicit p-wave term in the KN interaction. Preliminary fits showed that if only differential cross sections are used, then reasonably good fits are possible but, however, the calculated reaction and

total cross sections are smaller than the measured values by 30 to 50%. We have therefore used an extended input data set that included the differential cross sections for ^{6}Li and C together with the eight integral cross sections for ^{6}Li, C, Si and Ca at 714 MeV/c. As with the fits to only the integral cross sections, in these combined fits we have tried three different potentials: (i) a $t_{eff}\rho$ potential; (ii) an unconstrained DD potential; (iii) a constrained DD potential. In all cases the imaginary part included the rescaling discussed above. The normalization of the differential data was allowed to vary too, within the quoted range of $\pm 15\%$ [9]. The first two potentials produced good fits to the integral cross sections but only the unconstrained DD potential led, at the same time, also to a reasonably good fit to the differential data. The third potential, namely, the constrained DD potential that respects the low density limit, failed badly to reproduce simultaneously both types of data and also required an unacceptably large renormalization of the differential cross sections. In order to check the sensitivity of the results to the particular nuclear densities used in the optical potentials, the whole procedure was followed with both MAC and SP densities, as described above. The conclusions regarding the quality of the various fits remained unchanged.

Examples of the resulting real potentials for C are shown in Fig. 2. The continuous curves are for the unconstrained DD potential and the dashed curves are for the $t_{eff}\rho$ potential. Examples for the uncertainties, as obtained from the notch test mentioned above, are plotted for the unconstrained DD potential based on the MAC densities. These should represent also the uncertainties in the other potentials which are included in the figure. Also shown are the potentials obtained when the MAC densities are replaced by the SP densities and it is seen that although there are differences in details, the overall picture is the same for the two models. If, in the constrained fits, the parameter α is allowed to become negative, then better quality fits are obtained but the low density limit is no longer respected. The attractive 'pocket' near the nuclear surface, as seen in Fig. 2, persists. Comparing this figure with Fig. 1 it is seen that the real potential is a little better determined when the differential cross sections are included in the analysis. It is therefore concluded that the empirical potentials fail to respect the low density limit, at least within the present

parameterization. It is doubtful whether a more elaborate phenomenological real potential can be meaningfully derived from the present data.

V. RELATIVISTIC MEAN FIELD POTENTIALS

The Relativistic Mean Field (RMF) theory, treating nucleons as Dirac particles interacting via (large) scalar and vector fields, proved to be a valuable tool to describe nuclear structure and dynamics [27]. Extensions of the nuclear RMF theory to include hyperons are reviewed in Ref. [28]. In particular, the RMF approach has been applied to constructing the optical potential for elastic scattering of Λ and Σ hyperons on nuclei [29]. Therefore, the application of the RMF theory to K^+ – nucleus scattering seems to be a natural extension and, also, an interesting alternative to the phenomenological DD analysis. Furthermore, fitting the RMF potentials to K^+ – nucleus scattering data has the potential of providing information on the coupling of kaons to the meson fields involved, which is relevant for studying the behaviour of kaons in nuclear matter, particularly in connection to kaon condensation, and also for determining the equation of state of strange baryonic matter present in neutron stars [30].

In the RMF calculations reported below we used the common Lagrangian density in the nucleonic sector [27], with the linear parameterization of Horowitz and Serot [31]. For completeness, we also utilized the nonlinear model of Sharma et al. [32]. Kaons were incorporated into the RMF model by using kaon-nucleon interactions motivated by one boson exchange models. The simplest relevant form of the kaon-meson Lagrangian reads:

$$\mathcal{L}_K = \partial_\mu \overline{\psi} \partial^\mu \psi - m_K^2 \overline{\psi}\psi - g_{\sigma K} m_K \overline{\psi}\psi\sigma$$
$$-ig_{\omega K}(\overline{\psi}\partial_\mu\psi\omega^\mu - \psi\partial_\mu\overline{\psi}\omega^\mu) - ig_{\rho K}(\overline{\psi}\vec{\tau}\partial_\mu\psi\vec{\rho}^\mu - \psi\vec{\tau}\partial_\mu\overline{\psi}\vec{\rho}^\mu), \quad (9)$$

describing the interactions of kaons (ψ) with the scalar (σ) and vector (ω and ρ) fields. As was pointed out by Schaffner and Mishustin [30], this simple form has to be extended by the additional term

$$\mathcal{L}_{V^2} = (g_{\omega K}\omega_\mu + g_{\rho K}\vec{\tau}\vec{\rho}_\mu)^2\overline{\psi}\psi \tag{10}$$

in order to satisfy in the medium the Ward identity requiring coupling of the vector field to a conserved current. For isospin saturated nuclei, the equation of motion for the kaons reduces to:

$$[\partial_\mu\partial^\mu + m_K^2 + g_{\sigma K}m_K\sigma + 2ig_{\omega K}\omega_0\partial^0 - (g_{\omega K}\omega_0)^2]\psi = 0 \quad , \tag{11}$$

where ω_0 denotes the time component of the isoscalar vector field ω. It should be noted that the last (quadratic) term corresponding to $\mathcal{L}_{V^2}$ of Eq.(10) was omitted in the analysis of Section IV. We have checked the effects of the quadratic term ($\sim \omega_0^2$), as well as a possible extension by a term proportional to σ^2, and found these to be negligible. It is also possible to formulate the RMF calculations by reducing the second-order KG equation (11) into a Kemmer-Duffin-Petiau set of first-order coupled equations, as was done in Ref. [33].

The equation of motion can be expressed in the form of the KG equation (Eq.(1)) with the real part of the potential given by:

$$\text{Re } V_{opt} = \frac{m_K}{2\varepsilon_{red}^{(A)}}S + \frac{E_p}{\varepsilon_{red}^{(A)}}V \quad , \tag{12}$$

where $S = g_{\sigma K}\sigma$ and $V = g_{\omega K}\omega_0$. For the coupling constants $g_{\sigma K}$ and $g_{\omega K}$ we used the constituent quark model values [30,34], namely

$$\frac{g_{\sigma K}}{g_{\sigma N}} = \frac{g_{\omega K}}{g_{\omega N}} = \frac{1}{3} \quad . \tag{13}$$

In order to account for recoil effects we employed, following Ref. [35], the recoil corrections given by Cooper and Jennings [36], namely, we multiplied the scalar and vector potentials by the factors

$$R_S = \frac{M_A}{E_p + E_t}, \quad R_V = \frac{E_t}{E_p + E_t}. \tag{14}$$

Finally we introduced extra scaling coefficients for the scalar (C_S) and vector (C_V) potentials to be obtained from fits to the data. Using these scaling factors we aimed at tracing the energy dependence of the kaon couplings. After multiplying the S and V potentials in

Eq.(12) by R_S and R_V, and by C_S and C_V, respectively, we arrive at the expression for the real part of the optical potential V_{opt} to be used as a real potential in Eq.(1):

$$\text{Re } V_{opt} = \frac{m_K}{2E_p}\frac{M_A}{E_t}C_S S + C_V V. \tag{15}$$

The imaginary part of V_{opt} was again modified by letting Im $t_{eff}(\rho)$ depend linearly on the average density in excess of a threshold value (see Eq.(5)), with the same values of parameters β and ρ_{th} as in the case of the phenomenological potentials of Section II.

The fits of the RMF potentials were made by gridding on values of C_V and varying the coefficient C_S together with Im b_{eff}. This procedure was chosen because of the strong correlation between C_S and C_V. Searches stopped once reasonably low values of χ^2 (in our case $\chi^2 < 10$) were obtained. The results for the linear RMF parameterization [31] obtained from fits to the integral cross sections are summarized in Table V. It is seen that the scaling coefficients C_S and C_V decrease with increasing momentum, thus reducing significantly the contributions of both the scalar and vector potentials. Consequently, the resulting real part of V_{opt} is essentially consistent with zero at the highest momenta. Practically identical results (within the indicated errors) were obtained for the nonlinear RMF parameterization. When the differential cross sections are also included (only at 714 MeV/c), then the RMF best fits are significantly poorer than those obtained with the unconstrained DD potentials. The resulting RMF real potential does not have any attractive region, in contrast to the DD real potential. The fits based on the RMF approach thus confirm the empirical results concerning the real potential and in particular the loss of repulsion with increasing momentum. Note that this is opposite to the trend of Dirac-phenomenological nucleon optical potentials which become less attractive, even repulsive, with increasing energy [35].

VI. SUMMARY AND DISCUSSION

In the present work we have derived *self consistently* integral cross sections for K^+-nucleus interactions from transmission experiments [3–6], updating the procedure of Ref. [7]. These

reaction and total cross sections provide 32 data points for the study of medium effects in K^+ nuclear interactions. It had been realized for the total cross sections data subset [12–16], and quite recently also for the reaction cross sections data subset [7,19], that the values of these integral cross sections, for the relatively dense C, Si and Ca nuclei, exceed substantially the predictions of the first-order optical potential $V_{opt} = t\rho$, by up to about 25%. This is inconceivable [13] for as weakly interacting hadron as the K meson is. The free-space t matrix used in these theoretical studies, particularly its imaginary part which is proportional to the KN total cross section σ, is usually consistent with the total cross sections derived for the deuteron in the same transmission experiments [6,7].

In the eikonal approximation (cf. Ref. [13] for testing its validity at these energies), the total *reaction* cross section is given by

$$\sigma_R = \int d^2b \left(1 - \exp\left(-\frac{2}{\hbar v}\int_{-\infty}^{\infty} W\left(r\right) dz\right)\right) , \tag{16}$$

where $W(r) = -\,\mathrm{Im}\, V_{opt}(r)$. It is clear that, in order to increase the calculated value of σ_R, it is necessary to increase correspondingly $W(r)$ beyond the $t\rho$ expression $W_{opt}(r) = \hbar v \sigma \rho(r)/2$. Whereas a moderate increase of $W(r)$ (cf. the values of Im b_{eff} listed in Table II vs. the values Im b_0 listed there in parentheses) was found to satisfactorily reproduce the integral cross sections for ^{6}Li, no simple extension in terms of powers of the density ρ, or of the average density $\bar{\rho}$, could be found to reproduce simultaneously the integral data for the other, considerably denser nuclei. The only way found to reproduce self consistently all the integral cross sections was by introducing the density dependence of Eq. (5) according to which the (energy dependent) coefficient Im t_{eff} increases linearly with $(\bar{\rho} - \rho_{th})$ once $\bar{\rho} > \rho_{th}$, for a value of ρ_{th} given by Eq. (7) which is essentially independent of energy. Since, by fitting to the data, ρ_{th} turned out to be intermediate between $\bar{\rho}$ (^{6}Li) and $\bar{\rho}$ for the other heavier nuclei (cf. Table I), using this ad-hoc prescription for Im V_{opt} it is possible to bring the calculated C, Si and Ca integral cross sections into line with the ^{6}Li cross sections. It remains an open problem to understand the significance of this dependence and of this fitted value of ρ_{th} in terms of nonconventional reactive channels which might open up for $\bar{\rho} > \rho_{th}$.

For Re V_{opt} it was not necessary to introduce as complex density dependence as discussed above for Im V_{opt}. In fact, Re t_{eff} could be kept independent of density, becoming progressively less repulsive with energy, so that Re $V_{opt} \approx 0$ for $p \sim 700$ MeV/c. It was also possible to respect the low density limit, with a repulsive $t\rho$ term of about 25 MeV, by adding an attractive term depending on a higher power of the density such that the overall Re V_{opt} again becomes close to zero for $p \sim 700$ MeV/c. This same tendency of Re V_{opt} to become less repulsive with energy is also obtained when fits are based on RMF scalar and vector potentials taken from structure calculations or from nucleon-nucleus Dirac phenomenology. The RMF scaling factors C_S and C_V of Eq.(15) become vanishingly small with increasing energy, so that the (repulsive) vector and (attractive) scalar contributions at $p = 714$ MeV/c are individually small, of order 5 MeV for C, with a net repulsion given by their difference of about 5 MeV. It is interesting to note that for K^- nucleus scattering where the vector potential has the opposite sign, so that both S and V are then attractive, we would predict an attractive potential depth of about 10 MeV. Indeed, optical model fits [37] to K^- ^{12}C elastic scattering at $p = 800$ MeV/c [8] yield potential depths about 30 ± 6 MeV, depending on the geometry assumed for Re V_{opt}. This relatively weak attraction for $\bar{K}$ at intermediate energies is in stark contrast to the attraction of order 200 MeV felt by $\bar{K}$ mesons at low energies, as derived by fitting K^- atomic data [22].

We have also studied differential cross sections for elastic scattering of K^+ recently reported [9] for ^{6}Li and C at $p = 715$ MeV/c. Whereas these data definitely require a significant amount of density dependence beyond the $t\rho$ approximation in order to achieve reasonable good fits, the resultant potentials are incompatible with potentials obtained from fits to integral cross sections only. When fits to the combined data set at 714 MeV/c consisting of both differential and integral cross sections are made, Re V_{opt} is weakly repulsive within the nucleus, turning into an attractive pocket at the surface which, however, violates the low density limit. As for the fitted imaginary part of the optical potential, the specific density dependence of Eq. (5) is upheld also by this extended set of data.

A brief discussion of several theoretical works is in order. Siegel et al. [14] suggested

that nucleon "swelling" in the medium primarily affects the dominant S_{11} KN phase shift by increasing it in the nuclear medium. In the momentum range 500-700 MeV/c this amounts to increasing Im b_0, as required by the data, but *decreasing* (the negative) Re b_0 contrary to the trend suggested by fitting to the data, of increasing it to become less repulsive. A similar remark holds against the mechanism of dropping vector-meson masses in the nuclear medium as suggested by Brown et al. [15]. The meson exchange current effect considered in Refs. [17,18] is capable of producing the increment necessary for Im b_0 in order to fit the integral cross sections as function of energy, but it suggests no significant change in Re b_0. Finally, the most recent work by Caillon and Labarsouque [16], who consider medium effects for the mesons exchanged between the K^+ and the bound nucleons, produces *both* modifications required in order to fit the data, namely increasing Im b_0 and Re b_0 simultaneously to an extent which is comparable at 700 MeV/c with the values of b_{eff} shown in our Table II. However, these authors as well as other works are unable to produce the major medium effect which in our phenomenological approach is expressed by modifying Im b_{eff} by the $[1+\beta(\bar{\rho}-\rho_{th})\Theta(\bar{\rho}-\rho_{th})]$ factor. In this sense, no satisfactory theoretical approach yet exists to describe K^+ nucleus interaction at intermediate energies. We point out two features which make it even harder for theory to explain the integral cross sections data: (i) the self consistent values of σ_T published here are always larger, by about 5% than the previous values [6] used in some of the theoretical works; (ii) there exist now σ_R data, published here, which indicate a similar problem for theory as the σ_T data do. This appears to suggest that the theoretically missing part of the cross section belongs to some in-medium major reaction channels mistreated by the $t\rho$ optical model approach and its conventional, relatively minor modifications; or that at present theory misses some nonconventional in-medium effects that would strongly invalidate the $t\rho$ starting point.

New inelastic data for ^{6}Li and C at 635 and 715 MeV/c are being reported [10]. These inelastic excitations also require to be enhanced theoretically in order to fit the new data. Even though the corresponding transition densities peak at the nuclear surface where $\rho < \rho_{th}$, one cannot simply argue that these inelastic processes need not be strongly renormalized by

the medium effect specified here; ours is a *global*, not a local prescription, since it involves $\bar{\rho}$; not ρ. Of course, more work is needed to decide whether or not these inelastic cross sections shed new light on the problem of medium effects in K^+ nucleus interactions.

This research was partially supported by the Israel Science Foundation (E.F.), by the U.S.-Israel Binational Science Foundation (A.G.) and by the Grant Agency of the Czech Republic (J.M., grant No. 2020442). A.G. and E.F. acknowledge the hospitality of the Nuclear Physics Institute at Řež and J.M. acknowledges the hospitality of the Hebrew University.

REFERENCES

[1] C.B. Dover and G.E. Walker, Phys. Rep. 89 (1982) 1.

[2] D. Bugg et al., Phys. Rev. 168 (1968) 1466.

[3] Y. Mardor et al., Phys. Rev. Lett. 65 (1990) 2110.

[4] R.A. Krauss et al., Phys. Rev. C46 (1992) 655.

[5] R. Sawafta et al., Phys. Lett. B307 (1993) 293.

[6] R. Weiss et al., Phys. Rev. C49 (1994) 2569.

[7] E. Friedman et al., Phys. Rev. C55 (1997) 1304.

[8] D. Marlow et al., Phys. Rev. C25 (1982) 2619.

[9] R. Michael et al., Phys. Lett. B382 (1996) 29.

[10] R.E. Chrien, R. Sawafta, R.J. Peterson, R.A. Michael and E.V. Hungerford, Nucl. Phys. A (submitted 1997).

[11] C.M. Kormanyos et al., Phys. Rev. C51 (1995) 669.

[12] P.B. Siegel, W.B. Kaufmann and W.R. Gibbs, Phys. Rev. C30 (1984) 1256.

[13] C.M. Chen and D.J. Ernst, Phys. Rev. C45 (1992) 2011; M.F. Jiang, D.J. Ernst and C.M. Chen, Phys. Rev. C51 (1995) 857.

[14] P.B. Siegel, W.B. Kaufmann and W.R. Gibbs, Phys. Rev. C31 (1985) 2184.

[15] G.E. Brown, C.B. Dover, P.B. Siegel and W. Weise, Phys. Rev. Lett. 60 (1988) 2723.

[16] J.C. Caillon and J. Labarsouque, Phys. Rev. C45 (1992) 2503; Phys. Lett. B295 (1992) 21; Nucl. Phys. A572 (1994) 649; Nucl. Phys. A589 (1995) 609; Nucl. Phys. C53 (1996) 1993.

[17] M.F. Jiang and D.S. Koltun, Phys. Rev. C46 (1992) 2462.

[18] C. Garcia-Recio, J. Nieves and E. Oset, Phys. Rev. C51 (1995) 237.

[19] E. Friedman, A. Gal and J. Mareš, Phys. Lett. B396 (1997) 21.

[20] H. de Vries, C.W. de Jager and C. de Vries, At. Data Nucl. Data Tables 36 (1987) 495.

[21] M. Arima and K. Masutani, Phys. Rev. C47 (1993) 1325.

[22] E. Friedman, A. Gal and C.J. Batty, Phys. Lett. B308 (1993) 6; E. Friedman, A. Gal and C.J. Batty, Nucl. Phys. A579 (1994) 518.

[23] C.J. Batty, E. Friedman and A. Gal, Phys. Lett. B335 (1994) 273.

[24] J. Mareš, E. Friedman, A. Gal and B.K. Jennings, Nucl. Phys. A594 (1995) 311.

[25] C.B. Dover, J. Hüfner and R.H. Lemmer, Ann. Phys. [NY] 66 (1971) 248; J. Hüfner and C. Mahaux, Ann. Phys. [NY] 73 (1972) 525.

[26] E. Friedman, Few-Body Systems Suppl. 9 (1995) 97.

[27] B.D. Serot and J.D. Walecka, Adv. Nucl. Phys. 16 (1986) 1.

[28] J. Mareš and B.K. Jennings, Few-Body Systems Suppl. 9 (1995) 127.

[29] E.D. Cooper, B.K. Jennings and J. Mareš, Nucl. Phys. A580 (1994) 419.

[30] J. Schaffner and I.N. Mishustin, Phys. Rev. C53 (1996) 1416.

[31] C.J. Horowitz and B.D. Serot, Nucl. Phys. A368 (1981) 503.

[32] M.M. Sharma, M.A. Nagarajan and P. Ring, Phys. Lett. B312 (1993) 377.

[33] B.C. Clark, S. Hama, G.R. Kälbermann, R.L. Mercer and L. Ray, Phys. Rev. Lett. 55 (1985) 592.

[34] G.E. Brown and M. Rho, Nucl. Phys. A596 (1996) 503.

[35] E.D. Cooper, S. Hama, B.C. Clark and R.L. Mercer, Phys. Rev. C47 (1993) 297.

[36] E.D. Cooper and B.K. Jennings, Nucl. Phys. A483 (1988) 601.

[37] E.H. Auerbach, A.J. Baltz, C.B. Dover, A. Gal, S.H. Kahana, L. Ludeking and D.J. Millener, Ann. Phys. [NY] 148 (1983) 381.

FIGURES

FIG. 1. Real part for the K^+ carbon potential at 714 MeV/c from unconstrained DD fits to integral cross sections using MAC densities. The error bars are determined from notch tests (see text).

FIG. 2. Real part for the K^+ carbon potential at 714 MeV/c from fits to integral and differential cross sections. Continuous lines are for unconstrained DD potentials and dashed lines are for $t_{eff}\rho$ potentials. MAC and SP refer to the model used to calculate nuclear densities.

TABLES

TABLE I. Values of $\overline{\rho}$ (in units of fm^{-3}) obtained from SP calculations.

^{6}Li	C	Si	Ca
0.049	0.103	0.110	0.107

TABLE II. Fits to K^+ nucleus σ_R and σ_T values obtained by rescaling Im V_{opt} by the factor $1 + \beta(\overline{\rho} - \rho_{th})\Theta(\overline{\rho} - \rho_{th})$ with $\rho_{th} = 0.088$ fm^{-3}, $\beta = 13.0$ fm^3. Values in parentheses are for the free-space KN interaction parameter b_0. Values of χ^2 refer to the whole data base of 8 points at each momentum.

p (MeV/c)	Re b_{eff}(fm)	Im b_{eff}(fm)	χ^2
488	-0.154 ± 0.012	0.160 ± 0.002	0.5
	(-0.178)	(0.153)	
531	-0.119 ± 0.012	0.186 ± 0.002	10.3
	(-0.172)	(0.170)	
656	-0.035 ± 0.062	0.241 ± 0.002	2.1
	(-0.165)	(0.213)	
714	-0.044 ± 0.064	0.265 ± 0.001	7.8
	(-0.161)	(0.228)	

TABLE III. Reaction and total cross sections (in mb) for K^+ interaction with various nuclei from self consistent analysis of transmission measurements.

	reaction				total			
p (MeV/c)	^{6}Li	C	Si	Ca	^{6}Li	C	Si	Ca
488	67.8	128.4	276.2	362.5	77.5	165.4	373.7	503.2
	± 1.3	± 2.3	± 5.1	± 7.7	± 1.1	± 1.9	± 4.8	± 7.7
531	73.2	136.8	299.1	384.0	80.7	168.9	391.7	521.6
	± 0.8	± 1.4	± 3.4	± 4.5	± 0.7	± 1.3	± 3.3	± 4.4
656	79.0	148.2	311.8	408.6	86.4	179.5	403.2	548.8
	± 1.1	± 1.5	± 3.4	± 5.0	± 0.7	± 0.8	± 2.7	± 4.2
714	82.2	152.8	320.2	417.1	88.5	183.8	411.3	550.4
	± 1.2	± 1.5	± 3.6	± 5.5	± 0.6	± 0.9	± 2.3	± 2.8

TABLE IV. Re V_{opt} parameters (in fm) from density dependent fits to integral cross sections using MAC densities. Constrained fits are made to respect the low density limit.

	unconstrained			constrained		
p (MeV/c)	Re b_{eff}	Re B_0	χ^2	Re B_0	Re B_0+ Re b_0	χ^2
488	−0.175±0.034	0.033±0.054	0.2	0.029±0.014	−0.149±0.014	0.3
531	−0.093±0.049	−0.045±0.077	9.9	0.071±0.018	−0.101±0.018	11.2
656	0.077±0.068	−0.084±0.080	1.4	0.146±0.052	−0.019±0.052	2.2
714	0.046±0.087	−0.130±0.152	5.4	0.129±0.059	−0.032±0.059	10.4

TABLE V. Coefficients of the scalar (C_S) and vector (C_V) RMF potentials obtained from fits to the integral data. Also shown are the coefficient of the imaginary potential and the χ^2 of the fits.

p (MeV/c)	C_S	C_V	Im b_{eff}(fm)	χ^2
488	0.66±0.10	0.40±0.05	0.150±0.002	9.3
531	0.08±0.04	0.10±0.05	0.185±0.002	9.0
656	0.27±0.10	0.15±0.03	0.232±0.003	8.1
714	0.03±0.08	0.05±0.02	0.264±0.003	9.2

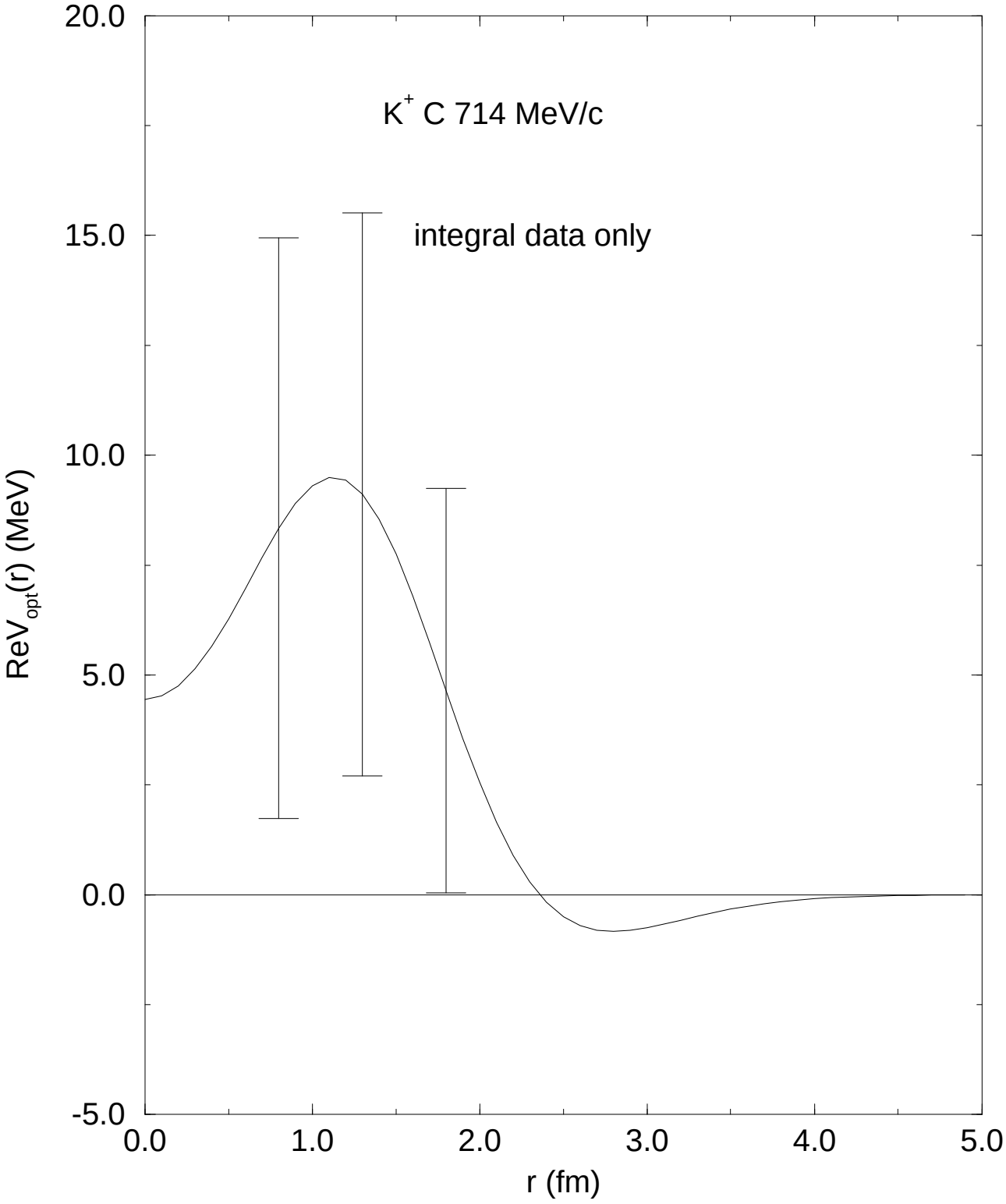
20.0
15.0
10.0
5.0
0.0
-5.0
0.0
1.0
2.0
3.0
4.0
5.0
K+ C 714 MeV/c
integral data only
ReVopt(r) (MeV)
r (fm)

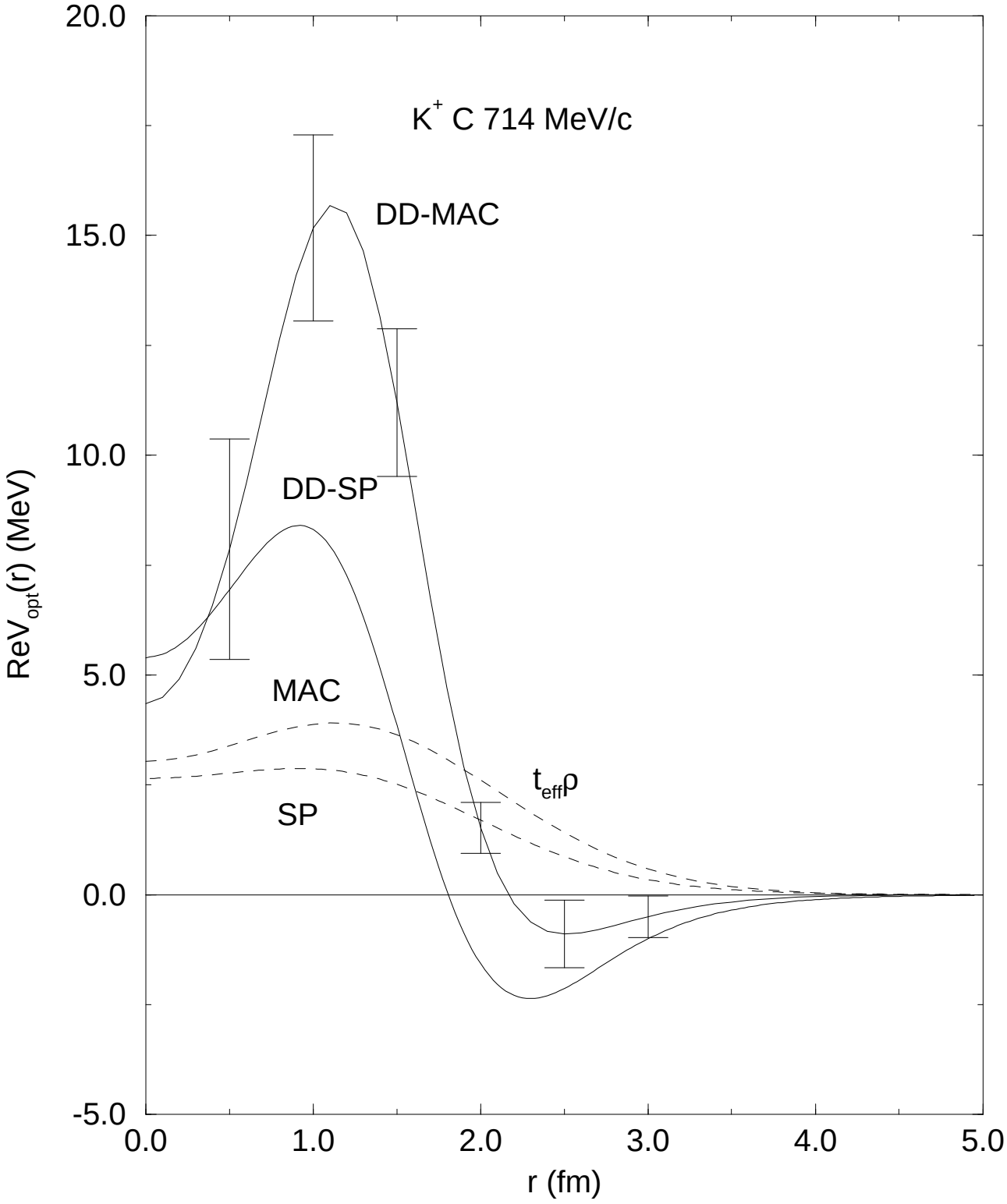
20.0
15.0
10.0
5.0
0.0
-5.0
0.0
1.0
2.0
3.0
4.0
5.0
ReV$_{opt}$(r) (MeV)
r (fm)
K$^+$ C 714 MeV/c
DD-MAC
DD-SP
MAC
SP
t$_{eff}$ρ